Summer Monsoon Rainfalls over Mid-Eastern China Lagged Correlated with Global SSTs

Yu Rucong (宇如聪)

LASG, Institute of Atmospheric Physics, Chinese Academy of Sciences, Beijing 100029

Zhang Minghua (张明华)

ITPA, MSRC, SUNY at Stony Brook, NY 11794-5000 *USA*

Yu Yongqiang (俞永强) and Liu Yimin (刘屹岷)

LASG, Institute of Atmospheric Physics, Chinese Academy of Sciences, Beijing 100029

(Received February 21, 2000; revised May 30, 2000)

ABSTRACT

Some features associated with Eastern China Precipitation (ECP), in terms of mean climatology, seasonal cycle, interannual variability are studied based on monthly rainfall data. The rainfall behavior over Eastern China has fine spatial structure in the seasonal variation and interannual variability. The revealed characteristics of ECP motivate us dividing Eastern China into four sub-regions to quantify significant lag-correlations of the rainfalls with global sea surface temperatures (SSTs) and to study the ocean's predominant role in forcing the eastern China summer monsoon rainfalls. Lagged correlations between the mid-eastern China summer monsoon rainfalls (MECSMRs) and the global SSTs, with SST leading to rainfall, are investigated. The most important key SST regions and leading times, in which SSTs are highly correlated with the MECSMRs, are selected. Part of the results confirms previous studies that show links between the MECSMRs and SSTs in the eastern equatorial Pacific associated with the El Nino – Southern Oscillation (ENSO) phenomenon. Other findings include the high lag correlations between the MECSMRs and the SSTs in the high and middle latitude Pacific Ocean and the Indian Ocean, even the SSTs over the Atlantic Ocean, with SST leading-time up to 4 years. Based on the selected SST regions, regression equations are developed by using the SSTs in these regions in respective leading time. The correlation coefficient between the observed rainfalls and regressed rainfalls is over 0.85. The root mean square error (RMSE) for regressed rainfall is around 65% of the standard deviation and about 15% of the mean rainfall. The regression equation has also been evaluated in a forecasting mode by using independent data. Discussion on the consistence of the SST-rainfall correlation with circulation field is also presented.

Key words: Summer monsoon, Rainfall, SST, Regression

1. Introduction

The Asian monsoon system, for its profoundly regional and global climate linkages, has been studied intensively (Webster and Yang, 1992; Yasunari and Seki, 1992; Meehl, 1994; Ju and Slingo, 1995; Soman and Slingo, 1997; Meehl and Arblaster, 1998; Webster et al., 1998), especially during the TOGA year (1985-1994). The broadly defined Asian monsoon actually consists of the Indian monsoon and the eastern Asian monsoon. The relationship between the Indian summer rainfall and the phase of El Niño – Southern Oscillation (ENSO) has been studied extensively (Rasmusson and Carpenter, 1983; Shukla and Paolino, 1983; Shukla and Mooley, 1987; Ju and Slingo, 1995; Harzallah and Sadourny, 1997). Drought years over India often accompany the warm phase of the central and eastern equatorial Pacific sea surface

temperatures (SSTs) (El Niño), and wet years often accompany the cold phase (La Niña). For the eastern Asian monsoon, with major part over eastern China, its relationships with ENSO and other large scale climate variability are more complex than those for the Indian monsoon due to the effect of complex geography of south Asia, the steep orography of the Tibetan Pleateau, and the sharp heating gradients.

The Asian summer monsoon is a major source of precipitation over eastern China. Precipitation patterns in China greatly depend upon monsoon activity. The summer monsoon rainfalls in China are affected by airflow originating from three systems. There are the southwest Indian summer monsoon, the cross–equatorial airflow over Southeast Asia and the South China Sea originating from the Australian region in the Southern Hemisphere, and the southeast monsoon coming from the southern flank of the subtropical high over the western Pacific. It is often observed that, from time to time, one of the monsoon airflow or a combination of them dominates the weather and precipitation pattern in China. The rainfall activity of the summer monsoon in China is a result of interaction of several monsoon systems. Most of the previous studies are focused on the links between the summer monsoon rainfall anomaly and sea surface temperature anomaly (SSTA) in the eastern equatorial Pacific, which was explained to link with subtropical high. Yet the behavior of the summer monsoon rainfall in China is likely to be a result of the nonlinear interaction of the separate components.

A number of studies have addressed these relationships of the eastern Asian monsoon with ENSO or the global climate variabilities (Lau and Li, 1984; Lau and Shen, 1988; Zhao et al., 1991; Shen and Lau, 1995; Ju and Slingo, 1995; Ose et al., 1997). Shen and Lau (1995) emphasized that the eastern Asian summer monsoon may be a part of a global scale biennial oscillation rhythm involving the interaction of monsoon rainfall, tropical SST and circulation.

In this study, based on the revelation of characteristics of eastern China summer rainfalls, we divide eastern China into four sub–regions to investigate the quantitative relationship between the rainfalls and the global SSTAs. The objective is to find useful long–term predictors from the SSTAs for the prediction of rainfalls. This paper is organized as follows. Section 2 describes the data. Section 3 presents the spatial and temporal precipitation characteristics and the regions of study in eastern China. Section 4 discusses the relationships between the rainfall anomalies and the SSTAs. Section 5 summarizes our results.

2. Data

The precipitation data used in this study are monthly station precipitation of 115 stations over eastern China from January 1951 to December 1998, which are compiled by China Meteorological Administration. The distribution of stations is shown in Fig.1.

The SST data used in this study are obtained by combining Da Silva's SST data set and Reynolds's SST data set. Da Silva's SST data (Da Silva et al., 1994) were derived from the Comprehensive Ocean–Atmosphere Data Set (COADS) from January 1945 to December 1989. Reynold's SST data were derived from in situ (ship and buoy) and satellite SST using optimum interpolation (Reynolds and Smith 1994) starting from 1982 to the present. The two sets of data were analyzed on 1° latitude by 1° longitude. The present study combines the Da Silva SSTs from 1945 to 1989 with the Reynolds SSTs from 1982 to the present. The combination is the weighting average of the two data sets from 1982 to 1989 with weights varying linearly from full weight on Da Silva's data in January 1982 to full weight on Reynolds's data in December 1989.

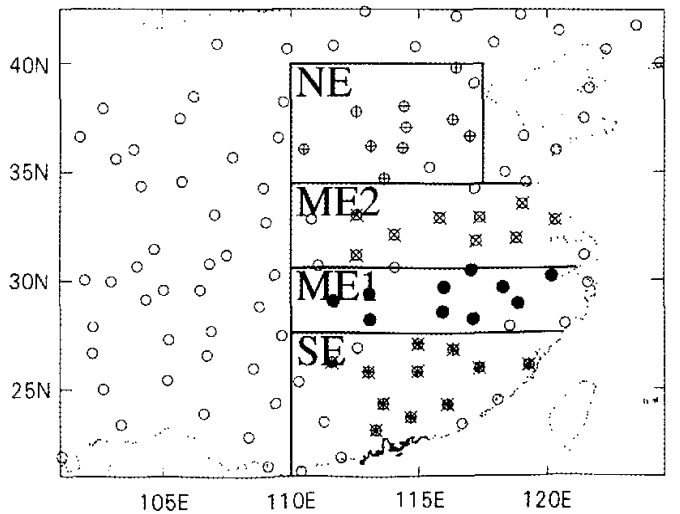

Fig. 1. The 115 station locations (circles) over eastern China with four divided subregions marked by heavy solid lines.

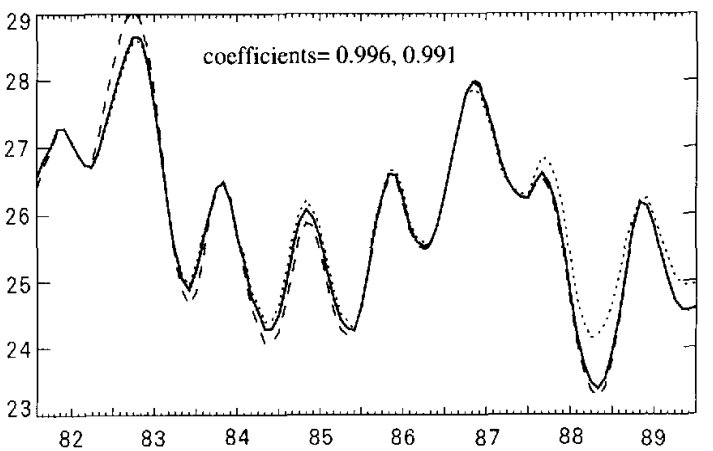

Fig. 2. The SSTs over the Niño3 region (5°S–5°N, 150°W–90°W) in the overlapping period for the Da Silva's SST dataset and Reynolds's SST dataset from 1982 to 1989. The solid line is the combined results, the dotted and dashed lines are from Da silva's data and Reynold's data respectively. Two correlation coefficients in the figure represent correlation of the solid line with the dotted line and with the dashed line respectively.

The compatibility of the two SST datasets over the overlapping period from 1982 to 1989 is checked for the SST climatology and the SST indices over various regions. Fig.2 shows the SSTs over the equatorial eastern Pacific (5°S–5°N, 150°W–90°W) in the overlapping period of two SST data sets from 1982 to 1989. The correlation coefficients in Fig. 2 represent the correlation of SST in combined result with SST in Da silva's data (0.996) and SST in Reynold's data (0.991) respectively.

The National Centers for Environmental Prediction (NCEP)/ A re–analysis data (Kalnay and Jenne, 1991; Kalnay et al., 1996) are used for discussion.

3. Climatological characteristics of Eastern China precipitation

The climatological rainfall amount in eastern China decreases from southeast toward northwest. The average annual rainfall amount is greater than 1600 mm in the southert part and less than 200 mm in the northern part. In the east of 110°E, the zonal distribution is the typical characteristic of rainfall belts over eastern China. For the seasonal variation, as we know, the summer monsoon is the major source of the rainfall. Following early spring rainfall, which occurs firstly over south of the Yangtze River, the summer monsoon rainfall belt forms from southeastern China and goes through two jumps northward around June and July. The rainfall belt moves rapidly southward, which marks the ending of the monsoon rainfall around the end of August.

Previous studies have shown that rainfall behavior of the eastern China summer monsoon has considerable spatial variability (Zhang 1988; Wu et al. 1995) due to interactions of several monsoon systems. The rotated Empirical Orthogonal Function (EOF) (Horel, 1981) analysis is used to identify the dominant modes of the interannual variability of the eastern China summer monsoon rainfall (ECSMR). The input consists of the summer rainfall anomalies averaged from April to August at each station. Fig. 3 shows the spatial patterns of the first four EOF modes. The first four modes explain about 40% of total variance, with the first mode accounting for 17% of the total variance.

Guided by the four EOF modes, eastern China is divided into four sub–regions in the following steps. The first step is to define the reference rainfall for each EOF mode by averaging rainfalls at five stations that have the first five maximal variances. In the following step, the sub–region, corresponding to one EOF mode, is determined by examining the correlation coefficients between the rainfall anomalies at each station and the reference rainfall anomalies. The sub–region consists of the stations in which the rainfall anomalies are highly correlated to the reference rainfall anomalies. The four sub–regions, corresponding to four EOF modes, are marked by solid lines in Fig.1 and named as SE, ME1, ME2 and NE respectively. In each of the four sub–region, the station circles are marked by "star" or "filled circle" or "cross" or "plus" respectively if the correlation coefficients between the rainfall anomalies of the station and its reference rainfall anomalies are over 0.7.

The rationality of above subdivision is checked, by examining the distinctions in the seasonal variation and the interannual variability expressed by the relationships between the monsoon rainfall anomalies and SSTAs over Niño3 (5°–5°N, 150°W–90°W) region. Fig.4 shows the monthly mean precipitation rates (MMPRs) at each sub–region respectively. The dark bars represent the MMPRs of sub–region mean, and the solid lines are the MMPRs at each station. The heavy horizontal solid and dashed lines represent the annual mean precipitation rates (AMPRs) and 1.5 times the AMPRs. It is clear that the seasonal variation of rainfalls at each sub–region is similar to that of sub–region mean. The seasonal variation between

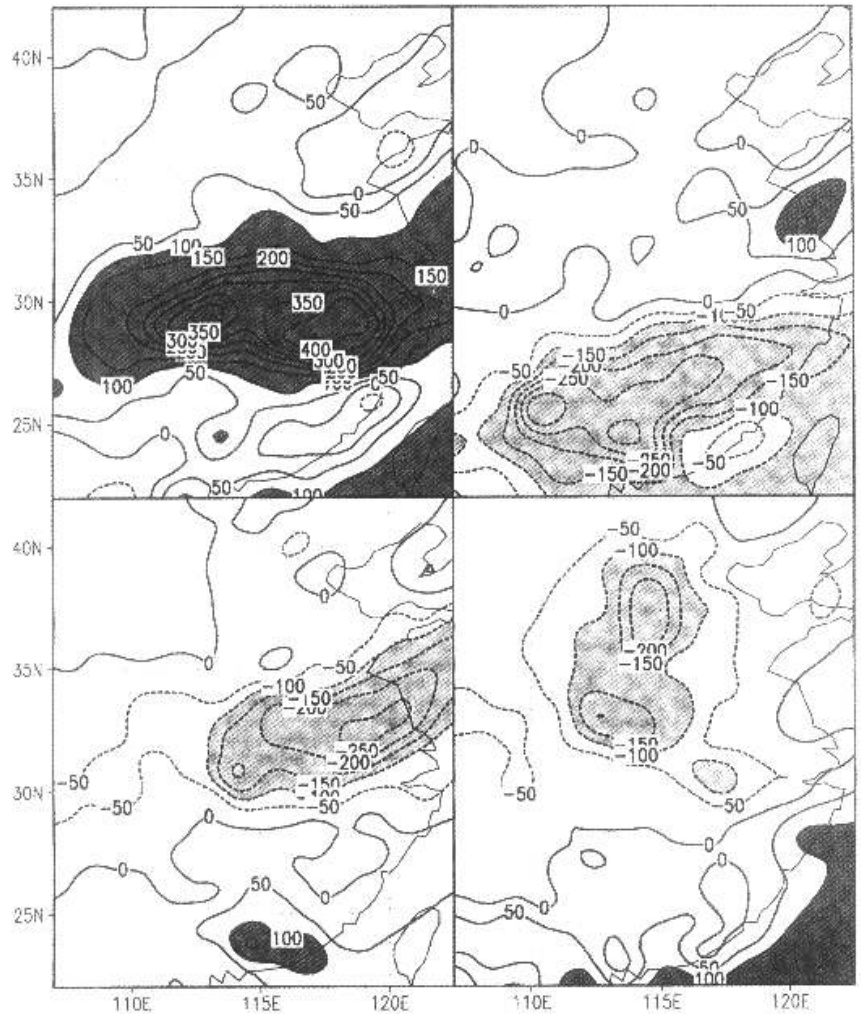

Fig. 3. Spatial patterns of the first EOF (upper left), second EOF (upper right), third EOF (lower left) and 4th EOF (lower right) modes of the eastern China summer monsoon rainfall (April to August averaged).

different sub-region is distinguished by the rainy season period or the period of onset and withdrawal of monsoon rain belt. The distinction of seasonal variation between the rainfalls in SE and ME1 is not as clear as that among others, but they are still to be distinguished by the variations of MMPRs from June to August. There is second peak of MMPR in SE in August because of typhoon rainfalls. The monsoon rainy season at each sub-region might be defined to include the months in which the MMPRs are over 1.5 times the AMPR or above the dashed line. From the south to north, the duration of the monsoon rainy season changes from April-May-June in SE and ME1, to June-July-August in ME2 and to July-August in NE.

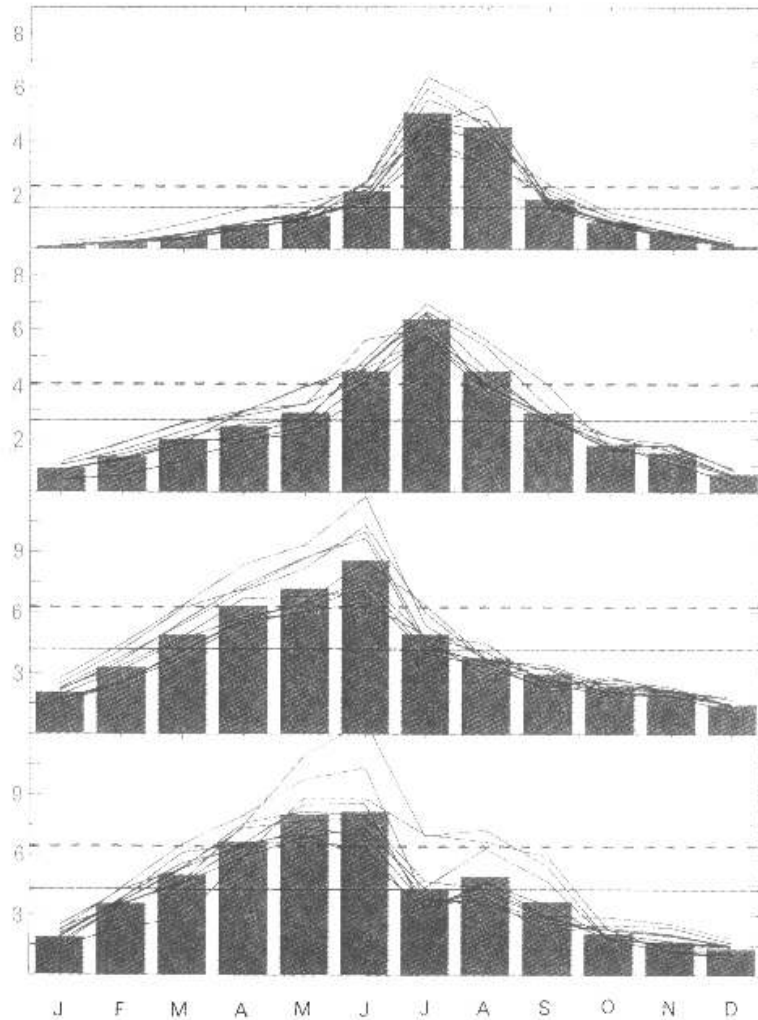

Fig. 4. The monthly mean precipitation rates (mm / day) in four sub-regions. From the uppermost panel to lowest panel, they correspond to the rainfall in NE, ME2, ME1 and SE respectively. The dark bars are the sub-region mean rates, and the solid lines are the rates at each station.

Fig. 5 shows the time-latitude sections of lag cross correlation between the SSTAs over Niño3 region and April to August zonal averaged ECSMRs on the latitudes from 22°N to 42°N. The longitudinal range is from 110°E to 120°E. The correlation coefficients are calculated by fixing the rainfall time series at each latitude from 1951 to 1997, and varying the SST time series from January of one year before the rainfall year to December of one year after the rainfall year. In the figure, Y0 denotes the rainfall year, Y−1 denotes one year before the rainfall year and Y+1 denotes one year after the rainfall year. There are several striking features.

One is the coherent structure of the lag correlation. For example, the figure exhibits significant leading time of up to one year (Y−1) of the eastern Pacific SSTA to the summer rainfall anomaly at 28°N and 31°N. On the other hand, there is also significant lead in the rainfall anomaly to the eastern Pacific SSTA (Y+1). This feature indicates the existence of temporal–spatial dynamic structure in the ECSMR and the ENSO. The second striking feature is the opposite sign of the correlation coefficients at the same lag time for different latitude belts. With lead year Y−1, the lag correlation exhibits a double see–saw pattern with positive correlation south of 31°N and north of 35°N with negative correlation in between. The third feature is that the double see–saw pattern is almost reversed with leading time occurring after the spring of the rainfall year. The lag correlation is very small in the spring, which is very reminiscent of the Latif and Graham observation–prediction correlation demise (Latif and Graham 1991) or the spring predictability barrier (Webster and Yang, 1992). This type of correlation pattern shows distinctive air–sea interaction between different sub–regions. The rainfall in SE has poor correlation with the SST in Niño3 region. There are similar rainfall–SST correlation patterns for the rainfall in NE and ME1, and a reversed pattern for the rainfall in ME2.

In summary, it is clear that the rainfall behavior over eastern China has fine spatial structure in the seasonal variation and interannual variability. Before studying the rainfall variation over eastern China in detail, it is indeed essential to divide eastern China into the four

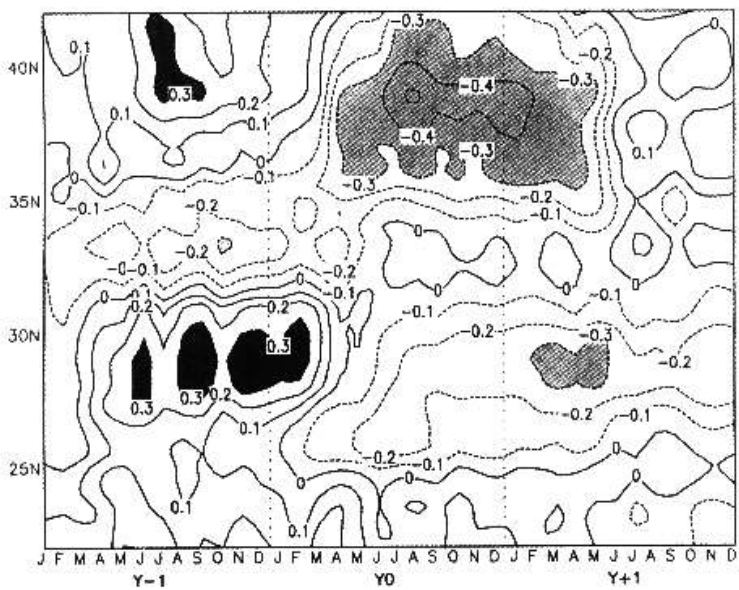

Fig. 5. The time–latitude sections of lag cross correlations between the SSTAs over Niño3 region (eastern equatorial Pacific) and April to August eastern China rainfall anomalies at each latitude, averaged from 110°E to 120°E, from 22.5°N to 42.5°N. Y0 denotes the rainfall year, Y−1 denotes one year before the rainfall year and Y+1 denotes one year after the rainfall year. Significant correlations at the 95% level are shaded.

sub–regions. In the next section, as an example, we will focus on the sub–region ME1 to study the lagged correlations between the rainfall anomalies and the SSTAs with focusing on SST leading. The sub–region ME1 corresponds to the first EOF mode with most significant interannual variability. The climatological rainfall amount in ME1 is well zonal distributed with northward decreasing clearly. Comparing with rainfalls over other sub–regions, from Fig. 5, yet the rainfall anomalies over ME1 are most significant correlated to SSTAs over Niñ o3 region with SST leading in preceding year. The sub–region ME1 is referred to as the mid–eastern China (MEC) as mentioned in the title of this study. The mid–eastern China summer monsoon rainfall (MECSMR) is our focus region in the following sections. For the sub–region NE, ME2 and SE, the same routine can be followed as that in ME1 to study their connections with SSTAs.

Fig.6 shows the normalized rainfall anomalies of MEC. The normalization is completed by their standard deviations, The dark bars represent the anomalies of regional averaged over MEC, and the solid lines are that at each station of MEC. As expected, the rainfall anomalies in most of stations have same sign as their mean in extreme flooding or drought years. From the Fig. 6, the fluctuation of rainfall in MEC is strong. The standard deviation of the rainfall in MEC is about 20% of the mean rainfall. There are about eight serious flooding years and nine serious drought years, in which the rainfall anomalies exceed 75% of the standard deviation, in the 48 years. The most extreme flooding event happened in 1954.

4. Correlation between MECSMR and global SST

In this section, we examine the quantitative lag cross correlations between the anomalies of MECSMR and the global SSTAs at each grid with SST leading time from January of Y–4 to the beginning of the summer rainy season. We select leading times and oceanic regions where the SSTAs are significantly and coherently correlated with the rainfall anomalies.

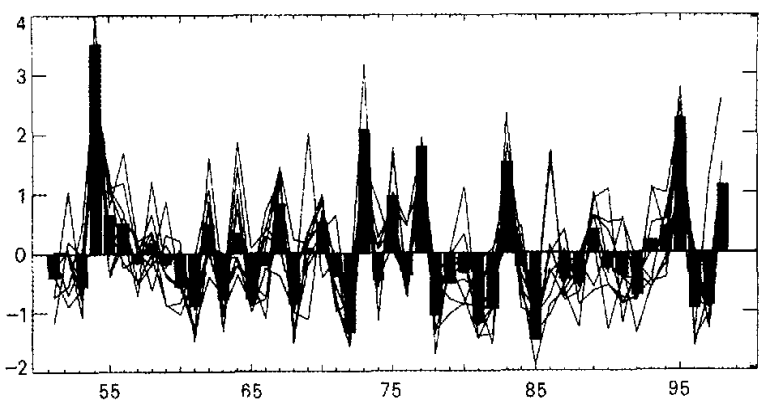

Fig. 6. The normalized rainfall anomalies during the monsoon rainy season in ME1. The normalization is completed by their standard deviations (134 mm). The dark bars represent the anomalies of mean rainfall over ME1, and the solid lines are the anomalies at each station.

These regions and leading times are then used to establish the regression equation of the rainfall to understand how the rainfall could be regressed or determined by the global SSTs.

4.1 *Lead correlated SST regions*

Major ocean regions, where SSTs are significantly and coherently correlated with the MECSMRs in respective leading time, can be found in Fig.7. In the figure, the contour lines

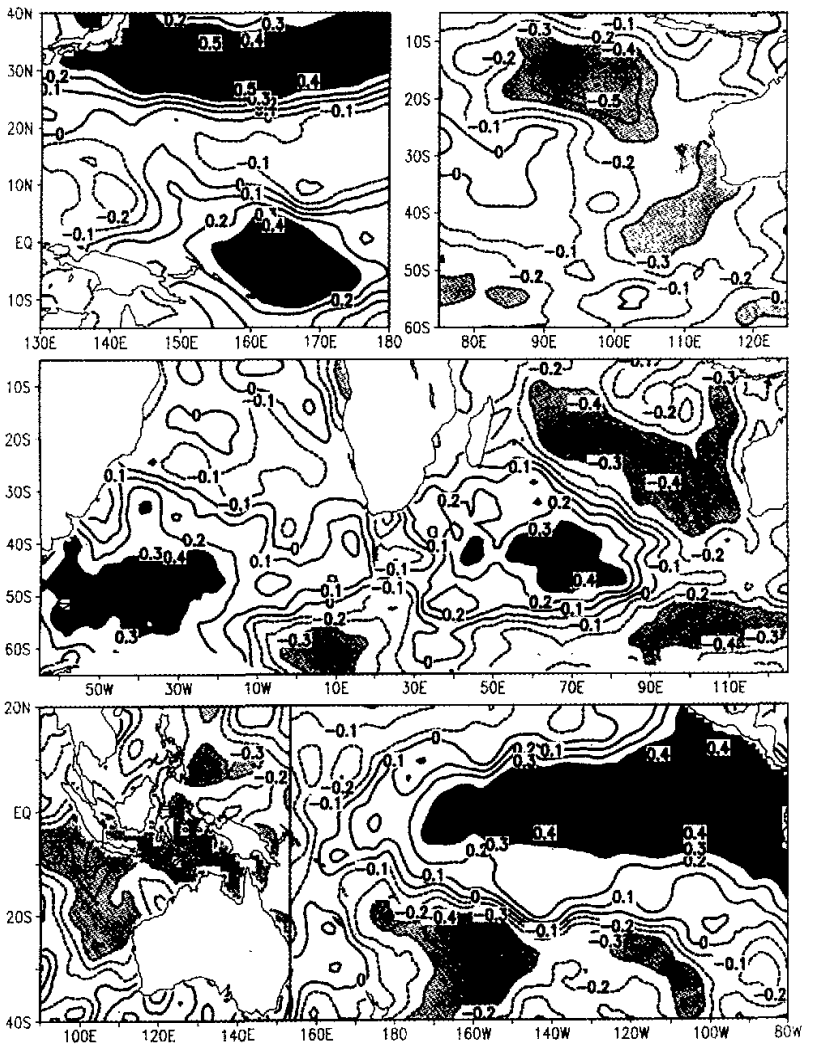

Fig. 7. The correlation coefficients between the rainfall anomaly over MEC and the SSTAs with SST leading in Y−4 (left−upper panel), with SST leading in the 4th preceding winter (right−upper panel), with SST leading in third preceding winter (middle panel), with SST leading in the spring of Y−1 (left−lower panel) and with SST leading from the summer of preceding year to the preceding winter (right−lower panel). Significant correlations at the 95% level are shaded.

are the lag correlation coefficients between averaged mean rainfall anomalies in MEC over the April to June and the SSTAs in the ocean grids with SST leading in specific times. The areas where the coefficients are larger than 0.3 or less than −0.3 are shaded. Correlation coefficient of 0.3 corresponds to the 95% significant level.

In the upper left panel of Fig.7, with SST leading time in March to October of Y−4 (four years before the rainfall year), the SSTAs over southeast warm pool and northern Pacific highly positively correlate with the rainfall anomalies in MEC. In the upper right panel and middle panel of Fig. 7, the SST leading times are in the fourth and third preceding winter respectively. In the lower left panel, the SST leading time is in the spring of Y−1. From the three panels, the SSTAs might keep negative anomalies about three years around the southeastern Indian Ocean or out of the Indonesian Throughflow before the flooding monsoon season in MEC happens. From the lower right panel, with the SST leading time from the summer of preceding year to the preceding winter, the result is consistent with previous studies that the rainfall anomalies in MEC might be related with the SST in the eastern Pacific in the preceding year.

Based on Fig. 7, seven specific ocean regions are finally selected and shown in Fig. 8. They are referred to as SSTR1 (labeled 1), SSTR2 (2), SSTR3 (3), SSTR4 (4), SSTR5 (5), SSTR6 (6) and SSTR7 (7) respectively. The SST leading times are in March to October of Y−4 over SSTR1 and SSTR2, in November of Y−3 to April of Y−2 over SSTR3, in November of Y−2 to January of Y−1 over SSTR4, in February to April of Y−1 over SSTR5, in July to September of Y−1 over SSTR6 and in Jun of Y−1 to February of Y0 over SSTR7. The SSTAs in the seven selected SST regions, with their respective leading time, are highly correlated with the rainfall anomalies in MEC as shown in Fig.9 and Fig.10. In Fig.9, the contour lines are the lag correlation coefficients between the rainfall anomalies at each station over eastern China and the mean SSTAs over seven selected SST regions with SST leading in specific times. Significant correlations at the 95% level are shaded. The temporal coherence of the correlation coefficients between the rainfall anomalies in MEC and the SSTA in the seven

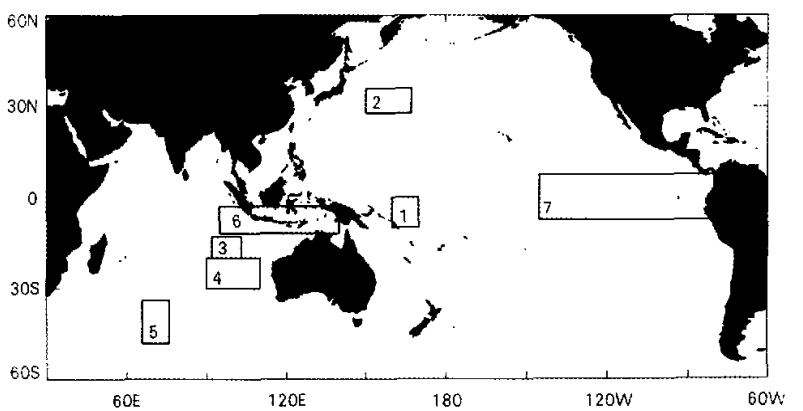

Fig. 8. Seven selected SST regions are marked by heavy solid rectangles and are named as SSTR1, SSTR2, SSTR3, SSTR4, SSTR5, SSTR6 and SSTR7 respectively.

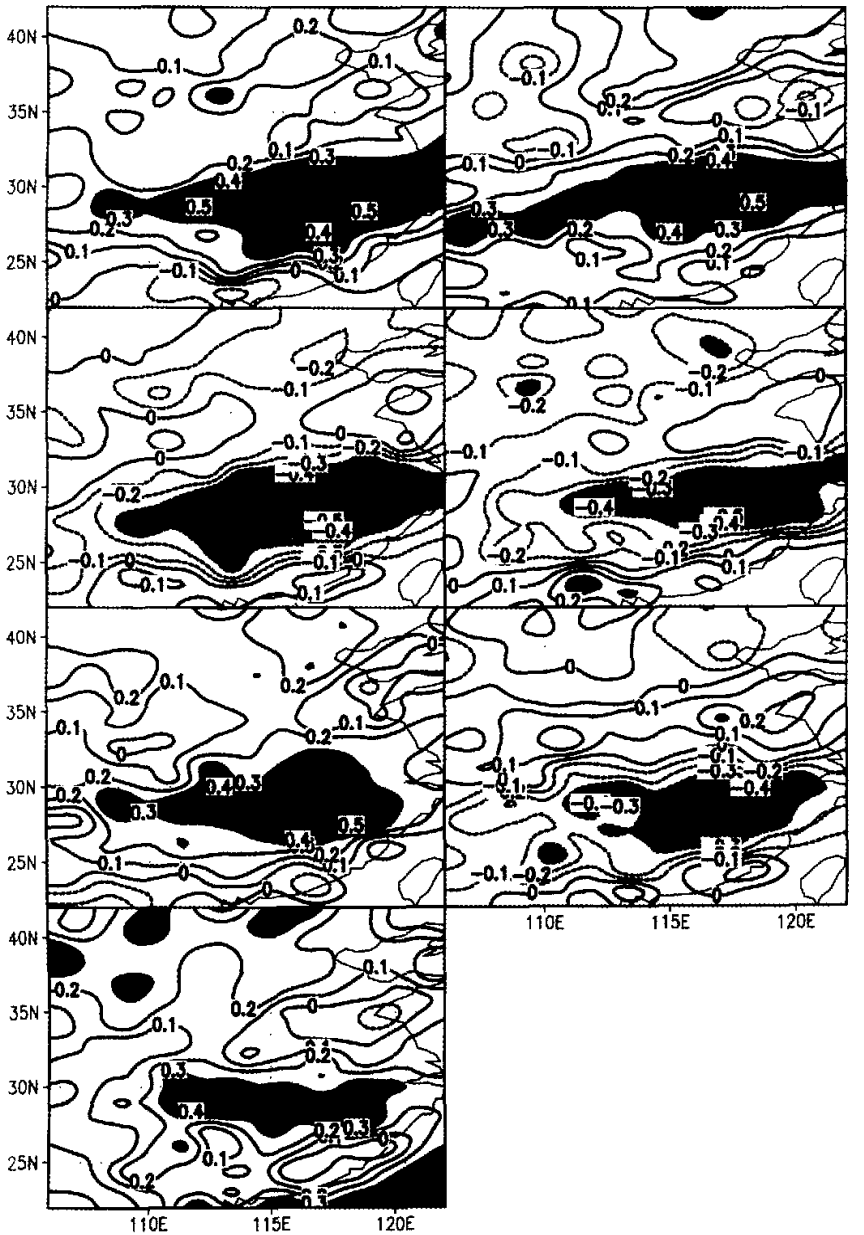

Fig. 9. The lag correlation coefficients between the anomalies of the monsoon rainfall at each station (averaged from April to August) and the SSTAs over seven selected SST regions with respective SST leading times. From left-upper panel, right-upper panel, to lowest panel, they are corresponding with SSTAs in SSTR1, SSTR2, to SSTR7. Significant correlations at the 95% level are shaded.

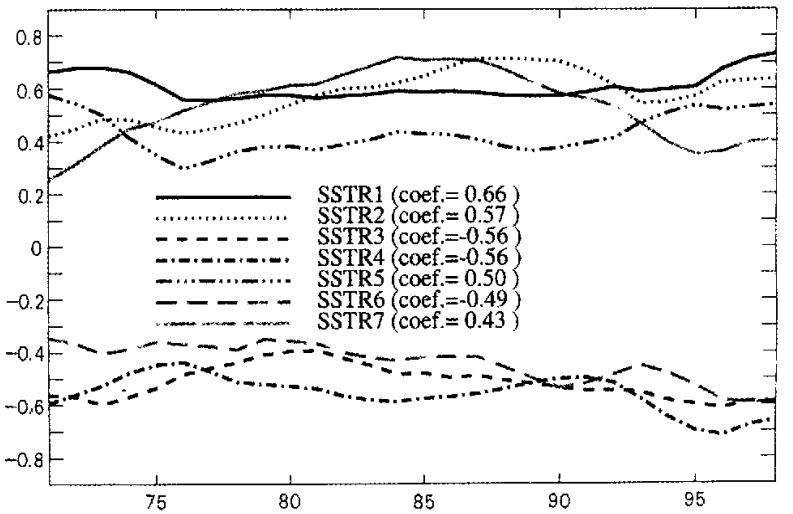

Fig. 10. The lag correlation coefficients of 21 years running correlating between the mean monsoon rainfall in MEC and mean SST in seven selected regions with their leading time. The first rainfall time series is from 1951 to 1971 and last rainfall time series is from 1978 to 1998. The labeled numbers are the correlation coefficients in full 48 years time series.

selected regions with their respective leading time is analyzed and shown in Fig. 10. In Fig. 10, the lines are the lag correlation coefficients of 21 year time series running correlating between the mean monsoon rainfall in MEC and mean SST in seven selected regions with their leading time. The first 21 year rainfall time series is from 1951 to 1971 and the last time series is from 1978 to 1998. As shown in Fig. 10, the correlation coefficients, in full 48 year time series, between the mean monsoon rainfall in MEC and mean SSTAs in the seven SST regions with their corresponding leading time are 0.66, 0.57, −0.56, −0.56, 0.50, −0.49, 0.43 respectively.

The present result is consistent with previous studies that the SST in the eastern Pacific in the preceding year is related with rainfall in the area around MEC. Yet, more significant and more spatial–temporal coherent correlated SST regions for rainfall in MEC are located in the western Pacific and the Indian Ocean, especially around the out of the Indonesian Throughflow, although their magnitudes of the SSTAs (or standard deviation) are much smaller than that in the eastern Pacific.

4.2 *Regression analysis*

A regression equation is developed by using the SSTAs in the selected regions in Fig. 8 in respective leading time mentioned in Section 4.1 to regress the summer monsoon rainfall. Fig. 11 shows the comparison between the regressed rainfall and observed rainfall. Fig. 11 shows the comparison between the regressed rainfall and observed rainfall. In the upper panel of Fig. 11, only SSTAs in SSTR1, SSTR2 and SSTR3 are used. This means that the shortest leading time of SST is two years. If we re–construct the regression equation to perform

regressing prediction, the prediction could be performed two years before the monsoon season. In the lower panel of Fig. 11, the SSTAs in the first six regions were used. The shortest time leading of SST is in preceding summer. The correlation coefficient between the regressed rainfall and observed rainfall in final regression is over 0.85. The root mean square (RMS) error of regressed rainfall for these 48 years is 87 mm, which is the amount of about 65% of the standard deviation (134 mm) and 13% of the mean rainfall (682 mm). It should be noted that not only many factors other than the SSTAs may affect the rainfall, but also the errors in SST and small-scale perturbations in the rainfall may affect the regression, and therefore, scatter around the regression line is expected.

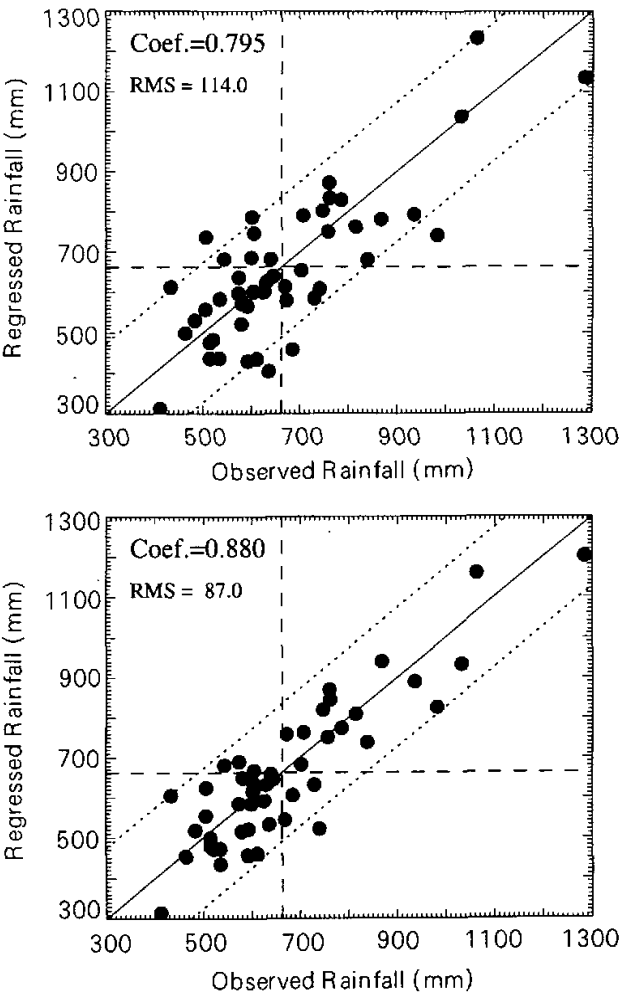

Fig. 11. The regressed rainfall and observed rainfall in MEC. The correlation coefficient and the root mean square (RMS) error are labeled.

To test the predictability of this kind of regression equation, starting from the 1976, using the SSTAs in first five selected regions, we re-construct the regression equation by using the preceding 25 years data only and forecast the rainfall in the current year for the last 23 years (1976 to 1998). The predicted results are shown in Fig.12. For the last 23 years, the correlation coefficient of the prediction with the observation reaches 0.829, and the RMS error for predicted rainfall is 96.5 mm.

5. Conclusion and discussion

In this study, the mean climatology, seasonal variation and interannual variability of rainfalls over eastern China have been studied by using the 1951–1998 monthly station rainfall data. The results show that the rainfall behavior has significant spatial and temporal variability with fine spatial structure in the seasonal variation and interannual variability. To study the rainfall variation over eastern China, eastern China has been divided into four sub-regions. The division is consistent with the distinctions in the season variation, rainy season duration, and interannual variability of rainfalls in each sub-region.

For one sub-region named MEC, we have selected seven ocean regions and the leading times where the SSTAs are significantly and coherently correlated with the monsoon season rainfalls in MEC. These regions and leading times have been used to establish the regression equation of the rainfall. The selected SST regions could be in the Indian Ocean, the Pacific and the Atlantic. The SSTAs which have more significant lag correlation with the rainfall anomalies are located in the western Pacific and southeastern Indian Ocean. The rainfalls can be regressed by using the selected SSTAs with leading time of one year to four years with significant skills. Comparing regressed rainfall with observed rainfall, the correlation coefficient can reach 0.88, and RMS errors are around 13% of the mean rainfall and 65% of the standard deviation.

We note that the correlation between two variables does not necessarily mean a causality relationship. It is possible that a third variable, which is unknown, is the cause of both. It is also likely that both of them take part in a global air–sea interactive climate system. From Fig. 5, significant lag cross correlations exist not only for SSTA leading the rainfall, but also for SSTA lagging the rainfall, which suggests that the SSTA and the rainfall anomaly in eastern China either interact directly with each other or participate in a large interaction system. No matter what the underlying physics is, the high lag correlation between SSTAs and the rainfall anomalies indicates that SSTAs might be used as useful predictors for the rainfalls, which is the principal goal of this paper.

It is indeed very difficulty to understand the physical linkage of the lag correlation between the rainfall anomalies in MEC and regional SSTAs with SST leading time up to four years. Competent coupled climate models might be useful tools to explore possible mechanism of linking the air–sea interactions related to the monsoon rainfall. But current climate models have difficulty in producing consistent simulations of precipitation in the eastern Asian monsoon regions. These models can not accurately simulate intraseasonal, annual and interannual variations, even the mean climatology of rainfall over eastern Asia. The sufficient monsoon specific model analysis and validation are essential in the future to have competent models for studying the physical linkage.

In order to have more confidence in accepting these lag correlations, we need to know if

the relationship between the rainfall and the SST is dynamically consistent with the circulation field. The composites of "wet–minus drought" (WMD) 500 hPa geopotential height (GH) anomalies during the summer monsoon rainy season have been computed by subtracting "drought" years composite from "wet" years composite. The "wet" and "drought" composites are obtained by averaging 500 hPa GH during summer monsoon period over four extreme flooding years (1973, 1977, 1983 and 1995) and four extreme drought years (1972, 1978, 1981 and 1985), with rainfall anomalies stronger than one standard deviation, respectively. The WMD composite is shown in Fig. 13. In the flooding year, 500 hPa geopotential height anomaly pattern includes a series of positive anomaly centers along high latitude of the Northern Hemisphere and subtropical latitudes of both hemispheres and negative anomaly centers along middle latitude of the Northern Hemisphere and high latitude of Southern Hemisphere. In all of the tropical area, the anomaly is positive. Yet, this kind of anomaly pattern indicates that the eastern China summer monsoon is highly correlated with global climate system. We calculated the lag correlations between the SSTAs in the seven selected SST regions and averaged 500 hPa GH anomalies at each grid during the monsoon season with SST time leading same as that leading to the rainfall to ensure that the circulation patterns related leading–times SSTAs are consistent with that in Fig. 13. Fig. 14 shows the lag correlation coefficients between the 500 hPa GH and SST in SSTR1 (upper panel) and SST in SSTR7(lower panel) with respective SST leading time. We were surprised by the upper panel of Fig. 14, in which the distribution of the correlation coefficient centers is very similar to the distribution of the anomaly center locations in Fig. 13. It means that the positive SSTA in SSTR1, southeastern warm pool, will indicate, in some degree, in four years late, having a special anomaly circulationpattern as in Fig. 13, correspondingly having a flooding summer monsoon season in MEC. The correlation patterns between SSTA in other selected regions and 500 hPa GH are not corresponding with the anomaly pattern in Fig. 13 as perfect as that in SSTR1, but correlation patterns in them indeed correspond with part of pattern in Fig.13. For example, in the lower panel of Fig.14, the correlation pattern between the SSTA in

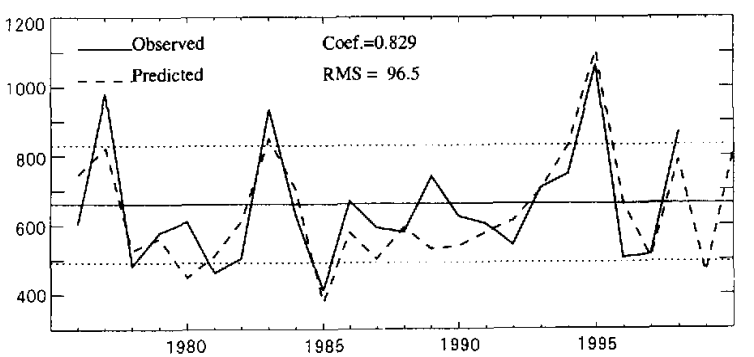

Fig. 12. The observed rainfall (solid line) and predicted rainfall (dashed line) in MEC. The correlation coefficient and the root mean square (RMS) error are labeled.

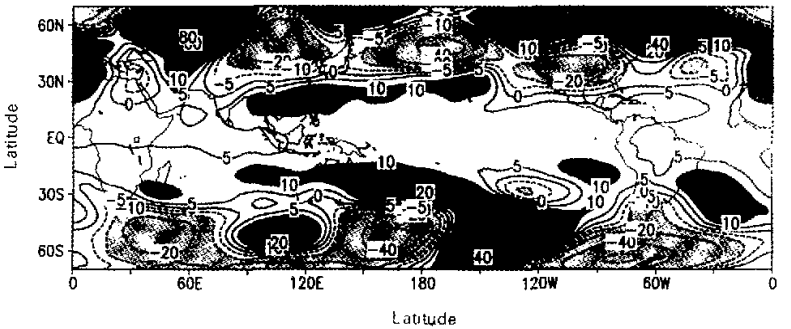

Fig. 13. The differences between April to June averaged 500 hPa geopotential heights over four extreme flooding years and that over four extreme drought years in units of ten geopotential meters (TGM). Contour interval is 5TGM. Values above 10 TGM are heavy shaded, and below −10 TGM are lightly shaded.

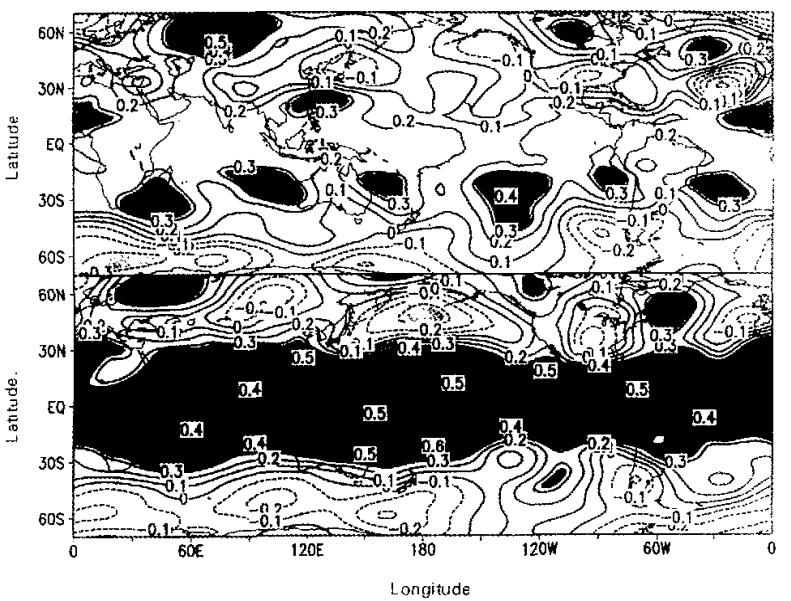

Fig. 14. The lag correlation coeffcients between April to June averaged 500 hPa Geopotential heights and SST in SSTR1 (upper panel), with SST leading time in Y−4, and SST in SSTR7 (lower panel) with SST leading time from summer of Y−1 to winter of Y0. Significant correlations at the 95% level are shaded.

SSTR7 and 500 hPa GH mainly corresponds with tropical and subtropical part of the pattern in Fig. 13. Therefore, it seems that the relationship between the rainfall and the SST is dynamically consistent with the circulation field.

It is hoped that the present study will provide some motivation for future modeling and observation studies concerning MECSMR. An examination of the performance of GCMs in simulating this observed interannual variability should help us to understand the mechanisms behind the observed relationships between the rainfalls and the SSTs. In this study, while keeping in mind that ENSO event is an important climate phenomenon, we also show that there are other important climate factors that can be used to address the regional prediction problem.

This work was jointed supported by Chinese Academy of Sciences under Grant " Hundred Talents" for " Validation of Coupled Climate models" and by U.S. Department of Energy under Grant DEFG0285ER 60314 to SUNY at Stony Brook. The authors are grateful to Professor R. D. Cess at SUNY, Stony Brook for his supports.

REFERENCES

Da Silva AM, C.C. Young, and S. Levitus, 1994: Atlas of Surface Marine Data 1994, Volume 1: Algorithms and Procedures. NOAA Atlas ENSDIS 6, U.S. Department of Commerce, NOAA, NESDIS, 1994.

Harzallah A. and, R. Sadourny, 1997: Observed lead–lag relationships between Indian summer monsoon and some meteorological variables. *Clim. Dyn.* **13**, 635–648.

Horel J.D., 1981: A rotated principal component analysis of the interannual variability of the Northern Hemisphere 500 hPa height field. *Mon. Wea. Rev.*, **109**, 2080–2092.

Huang Ronghui, and Y. Wu, 1989: The influence of ENSO on the summer climate change in China and its mechanisms. *Advances in Atmospheric Sciences*, **6**, 21–32.

Ju J., and J. Slingo, 1995: The Asian monsoon and ENSO. Quart. J. Roy. Meteorol. Soc., **121**, 1133–1168.

Kalnay E., and R. Jenne, 1991: Summary of the NMC / NCAR reanalysis workshop of April 1991. *Bull. Am. Meteorol. Soc.*, **72**,1897–1904.

Kalnay E., M. Kanamistsu, R. Kistler, W. Collins, D. Deaven, L. Gandin, M. Iredell, S. Saha, G. White, J. Woollen, Y. Zhu, M. Chelliah, W. Ebisuzaki, W. Higgins, J. Janowiak, K.C. Mo, C. Ropelewski, J. Wang, A. Leetmaa, R. Reynolds, R. Jenne, and D. Joseph, 1996: The NCEP / NCAR 40–year reanalysis project. *Bull. Am. Meteorol. Sci.*, **77**,437–471.

Latif M., and N.E. Graham, 1991: How much predictive skill is contained in the thermal structure of an OGCM ? TOGA Note, **2**, 6–8.

Lau K.M, G.J. Yang, and S. Shen, 1988: Seasonal and intraseasonal climatology of summer monsoon rainfall over East Asia. *Mon. Wea. Rev.*, **116**,18–37.

Lau K.M., and M. T. Li, 1984: The monsoon of East Asia and its global associations — A survey. *Bull Am. Meteorol. Soc.*, **65**,114–125.

Lau K.M., and P.J. Shen, 1988: Annual cycle, quasi–biennial oscillation, and Sourthern Oscillation in global precipitation. *J. Geophys. Res.*, **93**,10975–10988.

Meehl G.A., 1994: Influence of the land surface in the Asian summer monsoon: external conditions versus internal feedbacks. *J. Clim.*, **7**,1033–1049.

Meehl G.A., and J. M. Arblaster, 1998: The Asian–Australian monsoon and El Niño–Southern Oscillation in the NCAR Climate System Model. *J. Clim.*, **11**, 1356–1385.

Ose T, S. Yang, and A. Kitoh, 1997: Sea surface temperature in the South China Sea — an index for the Asian monsoon and ENSO system. *J. Meteorol. Soc. Japan*, **75**, 1091–1107.

Rasmusson M., and T. H. Carpenter, 1983: The relationship between eastern equatorial Pacific sea surface temperatures and rainfall over India and Sri Lanka. *Mon. Wea. Rev.*, **111**,517–528.

Reynolds R. W., and T. M. Smith, 1994: Improved Global Sea Surface Temperature Analyses Using Optimum In-

terpolation. *J. Clim.*, **7**,929–948.

Shen S., and K.M. Lau, 1995: Biennial oscillation associated with the East Asian summer monsoon and tropical sea surface temperature. *J. Meteorol. Soc. Japan*, **73**,105–124.

Shukla J., and D.A. Paolino, 1983: The Southern Oscillation and long range forecasting of the summer monsoon rainfall over India. *Mon. Wea. Rev.*, **111**,1830–1837.

Shukla J., and D. A. Mooley, 1987: Empirical prediction of the summer monsoon rainfall over India. *Mon. Wea. Rev.*, **115**,695–703.

Soman M. K., and J. Slingo, 1997: Sensitivity of the Asian summer monsoon to aspects of sea surface temperature anomalies in the tropical Pacific Ocean. *Quart. J. Roy. Meteorol. Soc.*, **123**,309–336.

Tian S.F., and T. Yasunari, 1992: Time and space structure of interannual variations in summer rainfall over China. *J. Meteorol. Soc. Japan*, **70**,585–596.

Van loon H., and S.L. Henry, 1986: Comments on warm events in the Southern Oscillation and local rainfall over southern Asia. *Mon. Wea. Rev.*, **114**,1419–1423.

Wang W.C., and K. Li, 1990: Precipitation fluctuation over semiarid region in northern China and the relationship with El Niño\Southern Oscillation. *J. Clim.*, **3**, 769–783.

Webster P. J., and S. Yang, 1992: Monsoon and ENSO : Selectively interactive systems. *Quart. J. Roy. Meteor. Soc.*, **118**, 877–926.

Webster P. J., V.O. Magana, T. N. Palmer, J. Shukla, R.A. Tomas, M. Yanai, T. Yasunari, 1998: Monsoon: Processes, predictability, and the prospects for prediction. *J. Geophys. Res.*, **103**,14451–14510.

Wu G.X., F.Y. Sun, J.F. Wang, X.C. Wang, 1995: Neibourhood response of rainfall to tropical sea surface temperature anomalies, Part II: Data analysis. *Chinese J. Atmos. Sci.*, **19**,663–676.

Yasunari T, and Y. Seki, 1992: Role of the Asian Monsoon on the interannual variability of the global climate system, J Meteorol Soc Japan. *Special edition on Asian Monsoon*, **70**,177–189.

Zhang J., 1988: *The Reconstruction of Climate in China for Historical Times*. Science Press, Beijing China, pp 79–82.

Zhao Z.G., Q.S. Liao, and X.Q. Li, 1991: ENSO and the weather in China. *Long-Range Forecasting Research Report*, No. 14 WMO / TD No.395.

长江流域夏季降水及其与海温的滞后相关

宇如聪　张明华　俞永强　刘屹岷

摘　要

基于月平均台站降水资料分析了中国东部降水的气候特征。由于其降水分布在空间和时间上的复杂性，为便于研究其与海温的关联，特别是海温对降水的影响，根据台站间降水变化在季节变化和年际变化以及与海温相关的一致性，将中国东部区域分成四个子区域。以长江流域的降水为代表，分析了海温对降水的超前相关。给出了主要影响海区和它们的超前时间。综合各影响海区海温和超前时间建立的回归方分析表明：回归降水和观测降水的相关系数大于 0.85。回归的平方根误差是其标准差的 60%和平均雨量的 15%。另外还分析了海温与降水相关与环流变化的一致性。

关键词： 夏季风，降水，海表温度，回归方程